tetrasaccharides in dichloromethane. After removal of dichloromethane, the mixture of organic QDs and blockwise alkylated tetrasaccharides was dried under a high vacuum. After the addition of PBS (pH 7.4) blockwise alkylated tetrasaccharide–organic QD complexes were successfully dispersed. Blockwise alkylated tetrasaccharides are amphiphilic. Alkylated part of tetrasaccharide derivatives has affinity with octyl groups of TOP and TOPO on the surface of QDs, resulting in the complex formation of amphiphilic tetrasaccharides and the organic QDs. Consequently, hydrophilic cellobiose or lactose parts of tetrasaccharide derivatives dissolved the organic QDs in water.

As shown in Fig. 1, the hydrodynamic diameter of the complexes was approximately 3.7 μm, indicating that the QDs did not disperse individually but aggregated with the blockwise alkylated tetrasaccharides. The layer of the blockwise alkylated tetrasaccharides (shell) and QDs (core) are included as the hydrodynamic diameter. We have reported water-soluble low molecular weight cellulose chains radially oriented on gold nanoparticles (Enomoto-Rogers et al. 2011). In this previous article, we have described that hydrodynamic diameters of gold nanoparticles covered by cellulose chains include those of gold core and cellulosic shell, confirmed by transmission electron microscopic observation.

As controls, an octyl β-D-glucopyranoside–organic QD complexes and organic QDs without additives were each dispersed in PBS separately and subjected to the same experiments; octyl β-D-glucopyranoside was chosen because it is a nonionic carbohydrate-based surfactant like the present blockwise alkylated oligosaccharides and is often used in biomedical research. The difference between our blockwise alkylated oligosaccharides and octyl β-D-glucopyranoside is the hydrophobic parts of the molecules. In the case of our new compounds, bulky alkylated cellobiosyl units serve as a hydrophobic moiety. By contrast, an aliphatic octyl group is hydrophobic in the commercially available octyl β-D-glucopyranoside. It is well known that the latter compound is ideal for the solubilization of membrane proteins but relatively cytotoxic. We thus compared the cytotoxicity of compounds **1–4** and octyl β-D-glucopyranoside toward human cell lines.

Cytotoxicity

Luminescent cell viability assay revealed that the IC_{50} of compound **1** was 1,300 μg/mL when U937 histocytoma cells were used as a representative human cell line. Moreover, the level of cytotoxicity exhibited by amphiphilic tetrasaccharides **1–4** was also evaluated by means of flow cytometry. When U937 cells were treated with amphiphilic compounds **1–4** (0.5 mg/mL)–QD (0.1 μM) complexes, most of the cells remained intact: specifically, 88.17, 87.71, 83.29, and 82.70% remained intact for compounds **1–4**, respectively, while 89.02% remained intact for a mock-treated control as shown in Fig. 2. In contrast, the octyl β-D-glucopyranoside (0.5 mg/mL)–QD (0.1 μM) complex exhibited a much higher level of cytotoxicity; only 29.51% cells were alive after treatment with the surfactant–QD complex. The cytotoxicity of compound **1**–QD complex against other human cell lines including Daudi, Raji, RPMI8226, J.RT3-T3.5, PEER, and MOLT3 is

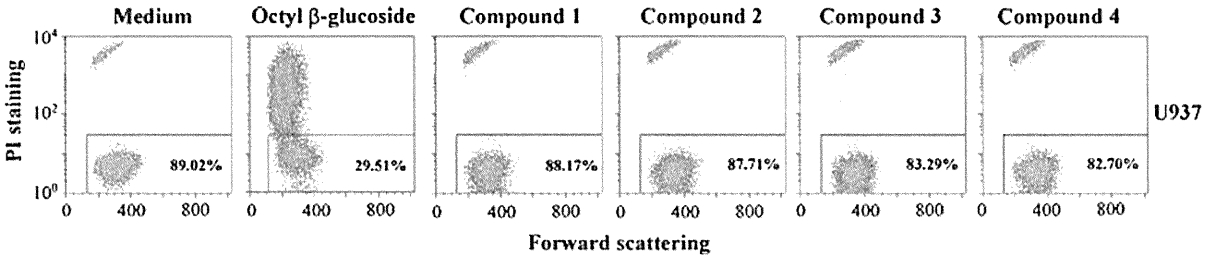

Fig. 2 Flow cytometric analysis of cell viability. U937 histocytoma cells were treated with the indicated compounds and stained with PI. The stock suspension consisted of 5 mg/mL of the newly synthesized saccharide and 1 μM of QDs in PBS. To 2 × 10^5 cells suspended in 45 μL of PBS was added 5 μL of the stock solution. The *horizontal axis* indicates the forward scattering, the intensity of which is proportional to the size of the cells. The *vertical axis* represents the incorporation of PI by dead cells. The lower cell populations enclosed by *lines* are thus live cells and the upper populations indicate dead cells

Table 1 Summary of cell viability (%) after treatment with various compounds

Cell lines	Medium	Octyl β-glucoside	1	2	3	4
U937	89.0	29.5	88.2	87.7	83.3	82.7
Daudi	88.0	43.8	88.0			
Raji	88.3	27.0	87.1			
RPMI8226	88.0	43.9	85.7			
J.RT3-T3.5	96.3	0.8	98.7			
PEER	98.0	6.5	99.5			
MOLT3	95.4	7.0	96.0			

Human lymphoma and myeloma cell lines were treated with the indicated compounds and cell viability (%) was determined by means of flow cytometry. 5 μL of the blockwise alkylated tetrasaccharides (5 mg/mL)–QD (1 μM) complexes in PBS were added to the suspension of human tumor cell lines at 2×10^5 cells in 45 μL of complete RPMI medium for each experiment. Errors were <±2.5%

summarized in Table 1. It is intriguing that compound **1**–QD complex was less toxic to T cell lymphomas than to B cell lymphomas and myelomas, while T cell lymphomas were significantly more sensitive to octyl β-D-glucopyranoside–QD complex. Because T cells play a cardinal role in immunity against microbial infections and malignancies, the present saccharides may serve as an ideal tool for T cell imaging in analyzing the complex immune system.

Labeling of live cells with blockwise alkylated tetrasaccharide–organic QD complexes

We next examined whether the newly prepared blockwise alkylated tetrasaccharide–organic QD complexes would interact with live cells. After U937 cells were incubated overnight with the QD complexes at final concentrations of 0.1, 0.2, and 0.5 mg/mL for the saccharides and 0.02, 0.05, and 0.1 μM for QD, the cells were labeled with QDs in a dose-dependent manner. As summarized in Table 1 and Fig. 3, methyl derivatives facilitated cell labeling more efficiently than their ethyl counterparts did in all conditions tested, while the structures of non-reducing end tetrasaccharides did not affect the cell labeling. The proportion of labeled cells increased with increasing the amount of blockwise alkylated tetrasaccharide–organic QD complexes.

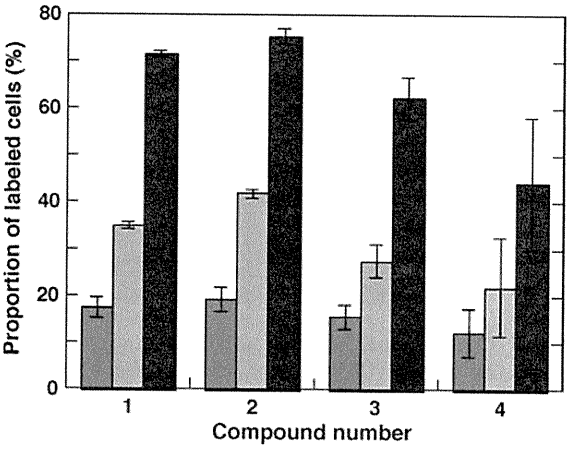

Fig. 3 Labeling of live cells with blockwise alkylated tetrasaccharide–organic QD complexes after 16 h. Each data point represents average of two independent experiments. The concentration of blockwise alkylated tetrasaccharides–QD complex is the same as that described in the legend of Fig. 2

Confocal laser scanning microscopic analysis of the interaction between blockwise alkylated tetrasaccharide–organic QD complexes and live cells

As described above, live cells were labeled with the newly prepared blockwise alkylated tetrasaccharide–organic QD complexes and analyzed by means of flow cytometry. It was difficult, however, to determine how the QD complexes interacted with live cells. We then employed confocal laser scanning microscopy to know the interaction between the QD complexes and live cells as shown in Fig. 4. After incubation of U937 with the QD complexes overnight, the cells were purified with a FACSAria cell sorter and viewed under a microscope. Typically, one or two QD complexes were simply attached to the surface of a U937 cell, as shown in Fig. 4.

Conclusion

Newly designed amphiphilic tetrasaccharide derivatives **1**–**4** spontaneously assembled to form micelle-like structures; blockwise alkylated tetrasaccharide–organic QD complexes were then successfully prepared. Based on the ATP-based U937 histocytoma cell viability assay, the IC_{50} of compound **1** was 1,300 μg/mL (1.70 mM), which was equivalent to those of food additives, cyclodextrins (α: 4,800 μg/mL: 4.93 mM,

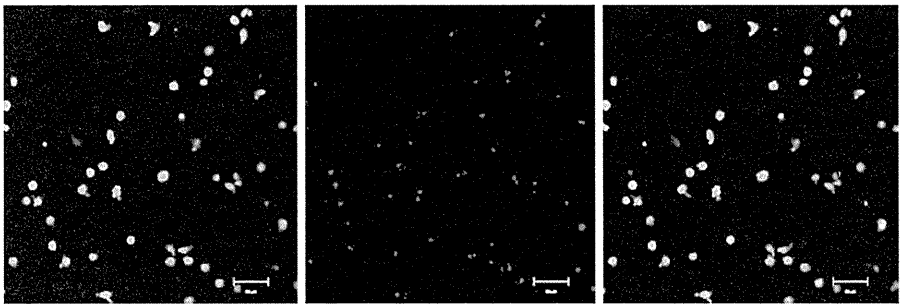

Fig. 4 Confocal laser scanning microscopic analysis of the interaction between U937 and the newly prepared compound **1**–organic QD complex. U937 cells visualized as *green fluorescence* (*left panel*); QDs as *red fluorescence* (*center panel*); a merged image (*right panel*). The *scale bar* indicates 50 μm. (Color figure online)

β: 1,200 μg/mL: 1.06 mM, and γ: 3,100 μg/mL: 2.39 mM; our unpublished data) and significantly lower than those of commonly used therapeutics like bisphosphonates (ca. 20 μM; our unpublished data). Flow cytometric analysis using lymphoma and myeloma cell lines revealed that the blockwise alkylated tetrasaccharide–organic QD complexes were less toxic than QDs encapsulated in octyl β-D-glucopyranoside, a widely used nonionic surfactant similar in structure to the blockwise alkylated tetrasaccharides (Kamitakahara et al. 2007, Nakagawa et al. 2011). On confocal microscopic and flow cytometric analyses, the blockwise alkylated tetrasaccharide–organic QD complexes attached to live cell surfaces of a variety of tumor cell lines. Owing to the tendency of QDs to aggregate, forming relatively large particles inside the micelle-like structures on the order of one micrometer in size, the fluorescent intensity of these complexes appeared to be relatively high. This may enable us to facilitate live cell imaging studies without using sophisticated apparatuses in preparation of the QD complexes, because the present QD complexes can be readily prepared in standard laboratories.

Acknowledgments This work was supported by Grants-in-Aid for Scientific Research from the Ministry of Education, Science, Culture, Sports, and Technology of Japan (MEXT) (to H.K. 21580205 and Y.T. 20590489), and by "Special Coordination Funds for Promoting Science and Technology" from MEXT and Astellas Pharma Inc. through the "Formation of Center for Innovation by Fusion of Advanced Technologies" program (to Y.T.).

References

Amvamzollo PH, Sinay P (1986) Streptococcus-pneumoniae type-Xiv polysaccharide—synthesis of a repeating branched tetrasaccharide with dioxa-type spacer-arms. Carbohydr Res 150(1):199–212

Buller GM, Zhang YZ, Godfrey WL (2007) Quantum dots as replacements for tandem dyes in flow cytometry. Cytom Part A 71A(9):766

Chen CS, Yao J, Durst RA (2006) Liposome encapsulation of fluorescent nanoparticles: quantum dots and silica nanoparticles. J Nanopart Res 8(6):1033–1038

Chen HL, Xue JL, Zhang YX, Zhu XB, Gao J, Yu BP (2009) Comparison of quantum dots immunofluorescence histochemistry and conventional immunohistochemistry for the detection of caveolin-1 and PCNA in the lung cancer tissue microarray. J Mol Histol 40(4):261–268

Cheyne RB, Moffitt MG (2007) Controllable organization of quantum dots into mesoscale wires and cables via interfacial block copolymer self-assembly. Macromolecules 40(6):2046–2057

Dean B, Oguchi H, Cai S, Otsuji E, Tashiro K, Hakomori S, Toyokuni T (1993) Synthesis of multivalent beta-lactosyl clusters as potential tumor-metastasis inhibitors. Carbohydr Res 245(2):175–192

DePasquale AC, Way AL (2009) Using quantum dots and flow cytometry in an attempt to identify adrenergic receptors on bovine sperm. Biol Reprod 151

Derfus AM, Chan WCW, Bhatia SN (2004) Intracellular delivery of quantum dots for live cell labeling and organelle tracking. Adv Mater 16(12):961–966

Dudu V, Ramcharan M, Gilchrist ML, Holland EC, Vazquez M (2008) Liposome delivery of quantum dots to the cytosol of live cells. J Nanosci Nanotechnol 8(5):2293–2300

Enomoto-Rogers Y, Kamitakahara H, Yoshinaga A, Takano T (2011) Water-soluble low-molecular-weight cellulose chains radially oriented on gold nanoparticles. Cellulose 18(4):929–936

Ferrari BC, Bergquist PL (2007) Quantum dots as alternatives to organic fluorophores for Cryptosporidium detection using conventional flow cytometry and specific monoclonal antibodies: lessons learned. Cytom Part A 71A(4):265–271

Ibanez-Peral R, Bergquist PL, Walter MR, Gibbs M, Goldys EM, Ferrari B (2008) Potential use of quantum dots in flow cytometry. Int J Mol Sci 9(12):2622–2638

Jaiswal JK, Mattoussi H, Mauro JM, Simon SM (2003) Long-term multiple color imaging of live cells using quantum dot bioconjugates. Nat Biotechnol 21(1):47–51

Kahn E, Menetrier F, Vejux A, Montange T, Dumas D, Riedinger JM, Frouin F, Tourneur Y, Brau F, Stoltz JF, Lizard G (2006a) Flow cytometry and spectral imaging multiphoton microscopy analysis of CD36 expression with quantum dots 605 of untreated and 7-ketocholesterol-treated human monocytic cells. Anal Quant Cytol 28(6): 316–330

Kahn E, Vejux A, Menetrier F, Maiza C, Hammann A, Grand ASL, Frouin F, Tourneur Y, Brau F, Riedinger JM, Steinmetz E, Todd-Pokropek A, Lizard G (2006b) Analysis of CD36 expression on human monocytic cells and atherosclerotic tissue sections with quantum dots—investigation by flow cytometry and spectral imaging microscopy. Anal Quant Cytol 28(1):14–26

Kamitakahara H, Nakatsubo F (2010) ABA- and BAB-triblock cooligomers of tri-O-methylated and unmodified cello-oligosaccharides: syntheses and structure-solubility relationship. Cellulose 17(1):173–186. doi:10.1007/S10570-009-9348-3

Kamitakahara H, Nakatsubo F, Klemm D (2006) Block co-oligomers of tri-O-methylated and unmodified cello-oligosaccharides as model compounds for methylcellulose and its dissolution/gelation behavior. Cellulose 13(4): 375–392

Kamitakahara H, Nakatsubo F, Klemm D (2007) New class of carbohydrate-based nonionic surfactants: diblock co-oligomers of tri-O-methylated and unmodified cello-oligosaccharides. Cellulose 14(5):513–528

Kamitakahara H, Yoshinaga A, Aono H, Nakatsubo F, Klemm D, Burchard W (2008) New approach to unravel the structure-property relationship of methylcellulose. Self-assembly of amphiphilic block-like methylated cello-oligosaccharides. Cellulose 15(6):797–801. doi:10.1007/s10570-008-9232-6

Kapoor V, Hakim FT, Rehman N, Gress RE, Telford WG (2009) Quantum dots thermal stability improves simultaneous phenotype-specific telomere length measurement by FISH-flow cytometry. J Immunol Methods 344(1):6–14

Kim J, Kim KS, Jiang G, Kang H, Kim S, Kim BS, Park MH, Hahn SK (2008) In vivo real-time bioimaging of hyaluronic acid derivatives using quantum dots. Biopolymers 89(12):1144–1153

Lei Y, Tang H, Yao L, Yu R, Feng M, Zou B (2008) Applications of mesenchymal stem cells labeled with Tat peptide conjugated quantum dots to cell tracking in mouse body. Bioconjug Chem 19(2):421–427

Nakagawa A, Kamitakahara H, Takano T (2011) Synthesis of blockwise alkylated (1 → 4) linked trisaccharides as surfactants: influence of configuration of anomeric position on their surface activities. Carbohydr Res 346(13): 1671–1683. doi:10.1016/j.carres.2011.04.034

Nida DL, Nitin N, Yu WW, Colvin VL, Richards-Kortum R (2008) Photostability of quantum dots with amphiphilic polymer-based passivation strategies. Nanotechnology 19(3)

Roederer M, Perfetto SP, Harper T, Bruchez M (2004) Quantum dots in flow cytometry. Cytom Part A 59A(1):148

Shi C, Zhou G, Zhu Y, Su Y, Cheng T, Zhau HE, Chung LWK (2008) Quantum dots-based multiplexed immunohistochemistry of protein expression in human prostate cancer cells. Eur J Histochem 52(2):127–133

Sun BQ, Xie WZ, Yi GS, Chen DP, Zhou YX, Cheng J (2001) Microminiaturized immunoassays using quantum dots as fluorescent label by laser confocal scanning fluorescence detection. J Immunol Methods 249(1–2):85–89

Urban FJ, Moore BS, Breitenbach R (1990) Synthesis of tigogenyl beta-O-cellobioside heptaacetate and glycoside tetraacetate via Schmidt trichloroacetimidate method—some new observations. Tetrahedron Lett 31(31): 4421–4424

Wu CH, Shi LX, Li QN, Jiang H, Selke M, Ba L, Wang XM (2010) Probing the dynamic effect of Cys-CdTe quantum dots toward cancer cells in vitro. Chem Res Toxicol 23(1):82–88. doi:10.1021/Tx900291c

Xing Y, Chaudry Q, Shen C, Kong KY, Zhau HE, Wchung L, Petros JA, O'Regan RM, Yezhelyev MV, Simons JW, Wang MD, Nie S (2007) Bioconjugated quantum dots for multiplexed and quantitative immunohistochemistry. Nat Protoc 2(5):1152–1165

Zrazhevskiy P, Sena M, Gao XH (2010) Designing multifunctional quantum dots for bioimaging, detection, and drug delivery. Chem Soc Rev 39(11):4326–4354

Cellulose (2011) 18:929–936
DOI 10.1007/s10570-011-9535-x

Water-soluble low-molecular-weight cellulose chains radially oriented on gold nanoparticles

Yukiko Enomoto-Rogers · Hiroshi Kamitakahara · Arata Yoshinaga · Toshiyuki Takano

Received: 1 December 2010 / Accepted: 25 March 2011 / Published online: 12 April 2011
© Springer Science+Business Media B.V. 2011

Abstract Cellulose chains bearing *N*-lipoyl group at the reducing-end as a sulfide linker, self-assembled on the surface of gold nanoparticles (CELL2Au, CELL13Au, and CELL41Au with the number average degrees of polymerization (DP_n) of 2, 13, and 41, respectively) were prepared. CELL2Au, CELL13Au, and CELL41Au were obtained via deprotection of the cellulose triacetate (CTA) self-assembled on the surface of gold nanoparticles that are consisting of CTA chains with corresponding DP_n organized in a radial manner with head-to-tail orientation, where a head is the reducing-end, and a tail is the non-reducing-end. CELL2Au and CELL13Au were well-dispersed in water including a trace of methanol, whereas CELL41Au was not. The transmission electron microscopy (TEM) observation of CELLAus deposited on copper grids revealed that the diameters (*d*) of the gold cores of CELL2Au, CELL13Au, and CELL41Au were 6.1, 6.1, and 11.5 nm, respectively. Wide angle X-ray diffractgram showed that cellulose chains of CELL13Au had quite low crystallinity and exhibited additional faint diffraction pattern of cellulose II. Cellulose chains of CELL41Au were amorphous. The UV–vis measurements revealed that CELL2Au and CELL13Au were well-dispersed in water. The hydrodynamic diameters (*D*) of CELL2Au and CELL13Au in water were 21.8 and 55.9 nm, respectively, according to dynamic light scattering (DLS) measurements, suggesting that cellulose chains on the gold were organized in a radial manner with head-to-tail orientation. ^{1}H-NMR measurement revealed that low-molecular-weight cellulose chains ($DP_n = 13$) on the gold dissolved in water, whereas low-molecular-weight cellulose ($DP_n = 13$) itself did not.

Keywords Low-molecular-weight cellulose · Reducing-end · Radial orientation · Water-soluble · Gold nanoparticles

Electronic supplementary material The online version of this article (doi:10.1007/s10570-011-9535-x) contains supplementary material, which is available to authorized users.

Y. Enomoto-Rogers · H. Kamitakahara (✉) · A. Yoshinaga · T. Takano
Division of Forest and Biomaterials Science, Graduate School of Agriculture, Kyoto University, Kitashirakawa-Oiwake-cho, Sakyo-ku, Kyoto 606-8502, Japan
e-mail: hkamitan@kais.kyoto-u.ac.jp

Introduction

Cellulose molecule has a hemiacetalic hydroxyl group at the reducing-end, which has different reactivity from other hydroxyl groups at C2, C3, and C6 positions. Focusing on the specific reactivity of the reducing-end, we have succeeded to prepare cellulosic diblock copolymers by introducing long-chain alkyl groups into the reducing-end of cellulose

chain (Kamitakahara et al. 2005; Kamitakahara and Nakatsubo 2005). Based on our synthetic strategy, we have studied the orientation and nano-structure of cellulose chains led by introduction of functional groups into their reducing-end. For example, we have recently prepared amphiphilic cellulose derivatives carrying hydrophobic alkyl group and pyrene group at the reducing-end, and have investigated self-assemble properties in NaOH aqueous solution (Enomoto et al. 2006). We have also prepared copolymers with cellulose side-chains (Enomoto-Rogers et al. 2009a, b). However, orientation or crystalline properties of cellulose chains in these cellulosic materials have not been investigated yet.

As a method to control the orientation of cellulose chains by immobilization of the reducing-end of cellulose, we have recently prepared cellulose triacetate (CTA) bearing a single disulfide group at the reducing-end, and succeeded in preparation of the CTA-self-assembled gold nanoparticles (CTAAu) (Enomoto-Rogers et al. 2010). CTA chains on the surface of gold nanoparticles were radially oriented in a head-to-tail manner, where a head is the reducing-end, and a tail is the non-reducing-end. The cellulose chains on the gold nanoparticles, which were obtained by deprotection of CTAAu, should be organized in a radial manner with head-to-tail orientation. Moreover, interchain distances of cellulosic chains on the gold nanoparticles (Enomoto-Rogers et al. 2010) were longer than crystalline lattice of cellulose I (Sugiyama et al. 1991; Woodcock and Sarko 1980) and cellulose II (Kolpak and Blackwell 1976). Meanwhile, it is well-known that cellulose is insoluble in water due to its crystalline structure formed via inter- and intra-molecular hydrogen bonding (Kamide et al. 1992). Only cello-oligosaccharides with the DP_n of up to ca. 7 are known to be soluble in water (Kobayashi et al. 1991) or in dimethyl sulfoxide (Isogai and Usuda 1991). To our knowledge, there have been no reports on radially oriented cellulosic materials. We anticipated that crystallinity and solubility of cellulose chains radially oriented on the gold nanoparticles might be different from free cellulose molecules, such as cellulose I or II.

In the present paper, we describe preparation of cellulose chains self-assembled on the surface of gold nanoparticles (CELL2Au, CELL13Au, and CELL41Au, degrees of polymerization (DP_n) cellulose of 2, 13, and 41, respectively) via deprotection of the cellulose triacetate (CTA)-self-assembled gold nanoparticles. Nanostructure and crystallinity of cellulose chains were also analyzed by transmission electron microscopy (TEM) and X-ray diffraction measurements. Water-solubility of cellulose chains on the surface of gold nanoparticles was analyzed in relationship to their degree of polymerization by means of UV–vis, dynamic light scattering (DLS), and NMR measurements are discussed in terms of crystallinity of cellulose chains.

Experimental

Materials

The gold nanoparticles grafted with cellulose triacetate (CTA) chains with the DP_n of 2, 13, and 41, were prepared as reported in our previous article (Enomoto-Rogers et al. 2010), and described as CTA2Au, CTA13Au, and CTA41Au, respectively. Cellohexaose was obtained from Seikagaku Cooperation (Tokyo, Japan). Low-molecular-weight cellulose ($DP_n = 15$) were prepared from cellulose microcrystalline (CF-11, Whatman) using phospholic acid according to previous articles (Atalla et al. 1984; Isogai and Usuda 1991). Low-molecular-weight cellulose ($DP_n = 13$) was prepared by deacetylation of cellulose triacetate ($DP_n = 13$). Sodium methoxide and all other reagents were commercially obtained and used without further purification.

Preparation of CELL2Au, CELL13Au, and CELL41Au nanoparticles

To a solution of CTA13Au (30.0 mg) in 20% methanol/chloroform (10.0 ml), sodium methoxide (0.2 mL) was added, and stirred for 1 h. The precipitated compounds were collected by centrifugation at 1,000 rpm for 3 min and washed by methanol. After methanol as supernatant was removed by decantation, the never-dried compounds in residual methanol were dissolved in water, and lyophilized, to obtain the dark purple solid, CELL13Au (14.3 mg). The same procedures were applied to CTA2Au and CTA41Au to obtain CELL2Au and CELL41Au, respectively. ^{1}H-NMR (CELL13Au) ($CDCl_3$): δ 3.35 (m, C2–H), 3.4–3.5 (m, C3–H,

C4–H, C5–H), 3.68 (dd, $J_{6a,\ 6b} = 11.6$, $J_{5,\ 6} = 4.0$, C6–H_a), 3.83 (d, $J_{6a,\ 6b} = 10.0$, C6–H_b), 4.38 (d, $J_{1,\ 2} = 8.0$, C1–H).

FT-IR measurements

Fourier transform infrared (FT-IR) spectra were recorded on a Shimadzu FTIR-4000 spectrophotometer equipped with an ATR attachment (Durasampl IR II).

TEM analysis

Transmission electron microscopy (TEM) images were collected by a JEOL JEM-1220 system operating at an accelerating voltage of 100 kV. Samples were prepared by depositing CELLAu dispersed in water (0.1 mg/mL, 10 μL) on copper grids that were pre-coated by Formvar (polyvinyl formal). The samples were stained with uranyl diacetate. The sizes of particles were calibrated using Latex Particles ϕ 0.23 μm (Ohken Shoji, Japan). TEM images were recorded on Fuji FG films (Fuji Film, Japan). The image data of the films were printed on photographic papers at 6.3 magnifications. The developed images were stored with a general scanner at 300 dpi. TEM images were analyzed using public domain ImageJ program (Rasband, W.S., US National Institutes of Health, Bethesda, Maryland, USA, http://www.rsb.info.nih.gov/ij/, 1997–2009). The diameters (d) of the gold cores were obtained from measurements of at least 100 particles per sample.

X-ray diffraction measurements

X-ray diffraction measurements were carried out with a Rigaku diffractometer Ultima IV. A Nickel-filtered CuKα radiation was used at 40 kV and 30 mA. Samples were prepared by lyophilization of never-dried CELLAu dispersed in water. Low-molecular-weight cellulose ($DP_n = 15$) was used to obtain reflection pattern of cellulose II.

UV–vis measurements

UV–vis spectra were recorded on a JASCO V-560 spectrometer at 25 °C. CELL2Au and CELL13Au dispersed in water (0.1 mg/mL) were filtered with poly(tetrafluoroethylene) syringe filter (pore size of 0.2 μm) before the measurement.

DLS Measurements

Hydrodynamic diameters of gold nanoparticles coated by cellulose chains were recorded on dynamic light scattering (DLS) spectrophotometer (ELS-Z2, Photal Otsuka Electronics) equipped with He–Ne laser ($\lambda = 632.8$ nm) at 25 °C. Hydrodynamic diameters were obtained by Cumulant method. Intensity and number size distributions were obtained by Marquardt method (Gulari et al. 1979). CELL2Au and CELL13Au dispersed in water (1 mg/mL) were filtered with hydrophilic PTFE syringe filter (pore size of 0.2 μm) before the measurement.

NMR measurements

^{1}H-NMR spectra were recorded on a JEOL JNM-A500 FT-NMR (500 MHz) spectrometer in D_2O. Chemical shifts (δ) and coupling constants (J) are reported in (ppm) and (Hz), respectively. The precipitated CELL13Au obtained after deacetylation of CTA13Au was collected by centrifugation at 1,000 rpm for 3 min and washed by methanol-d_4. After methanol as supernatant was removed by decantation, the never-dried CELL13Au in residual methanol was dissolved in D_2O.

Results and discussion

Preparation of cellulose chains self-assembled on the surface of gold nanoparticles

CTA-self-assembled gold nanoparticles, CTA2Au, CTA13Au, and CTA41Au, were treated with sodium methoxide, resulting in the formation of cellulose chains self-assembled on the surface of gold nanoparticles, CELL2Au CELL13Au, and CELL41Au, respectively, as described in Fig. 1. Sodium methoxide was chosen as a reagent for deacetylation because no peak was observed in the X-ray diffractograms of the deacetylated compounds when 1,8-diazabicyclo[5,4,0]-7-undecene (DBU) was used (data not shown). The completion of deacetylation was confirmed by FT-IR spectra, as shown in Fig. 2. An absorbance of carbonyl (C=O) group at 1,760 cm^{-1}

completely disappeared for CTA13Au, and a strong OH absorbance at $\nu = 3{,}342\ cm^{-1}$ appeared for CELL13Au, indicating that deacetylation proceeded completely, and that cellulose chains remained on the gold nanoparticles. Interestingly never-dried CELL2Au and CELL13Au nanoparticles, which are in residual methanol after workup procedures, were well-dispersed in water at least for a week, whereas CELL41Au nanoparticles were not.

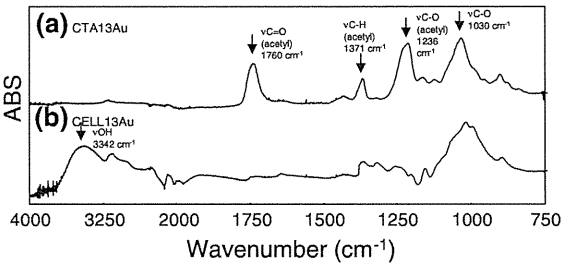

Fig. 2 FT-IR spectra of **a** CTA13Au and **b** CELL13Au

TEM observations

The CELLAu nanoparticles in dry state were analyzed by transmission electron microscopy (TEM). Specimens for TEM observation were prepared by depositing CELLAu nanoparticles dispersed in water on Formvar-pre-coated copper grids. The TEM images of gold nanoparticles, and the size distributions of the diameters (*d*), are shown in Fig. 3. The characteristics of original CTAAu and CELLAu nanoparticles are listed in Table 1. The *d*s of the gold cores of CELL2Au, CELL13Au, and CELL41Au were 6.1, 6.1, and 11.5 nm, respectively. The *d*s of the gold cores of CTA2Au, CTA13Au, and CTA41Au were 8.7, 7.9, and 13.4 nm, respectively, according to our previous work (Enomoto-Rogers et al. 2010). The *d*s and its standard deviations showed no substantial difference before and after deacetylation, indicating that the gold nanoparticles were stable under alkaline condition. In the case of CTAAu nanoparticles, the interparticle distance between nanoparticles agreed well with CTA molecular chain length (Enomoto-Rogers et al. 2010). However, in the case of CELLAu nanoparticles prepared in this work, the interparticle distances were irregular and could not be controlled by chain length of cellulose molecule. CELLAu nanoparticles tended to aggregate and it was hard to measure interparticle distances. It is likely due to strong interactions between cellulose chains such as hydrogen bonding. The same phenomenon has been observed in the case of cellulose nanocrystals. Cellulose nanocrystals or particles with free hydroxyl groups formed aggregate in water via Van der Waals interaction or hydrogen bonding (Wang et al. 2008, 2007). Cellulose layer was not observed even when they were stained with uranyl acetate, probably because crystallization of cellulose chains was inhibited by covalent bonding between sulfur atom and gold surface with wider interchain distances compared to crystal lattices of cellulose I or cellulose II, as discussed in following section.

X-ray diffraction measurements

In X-ray diffractgrams of CELL13Au and CELL41Au nanoparticles, a strong reflection assigned to Au (111) (Qazi et al. 2009; Wang et al. 2003) were observed, as shown in Fig. 4a and b. CELL13Au showed the quite weak reflections peaks assigned to cellulose II (110) and (200), as shown in Fig. 4a and c (Isogai et al. 1989). Regarding the crystalline structure, there are some possibilities for the structures of cellulose chains, because self-assembled structures in solid state could not be investigated in detail. Parallel cellulose chains might show diffraction pattern of

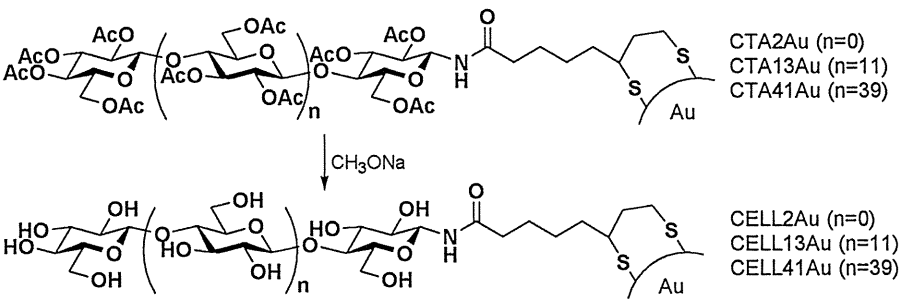

Fig. 1 Preparation of cellulose chains self-assembled on the surface of gold nanoparticles, CELL2Au, CELL13Au, and CELL41Au

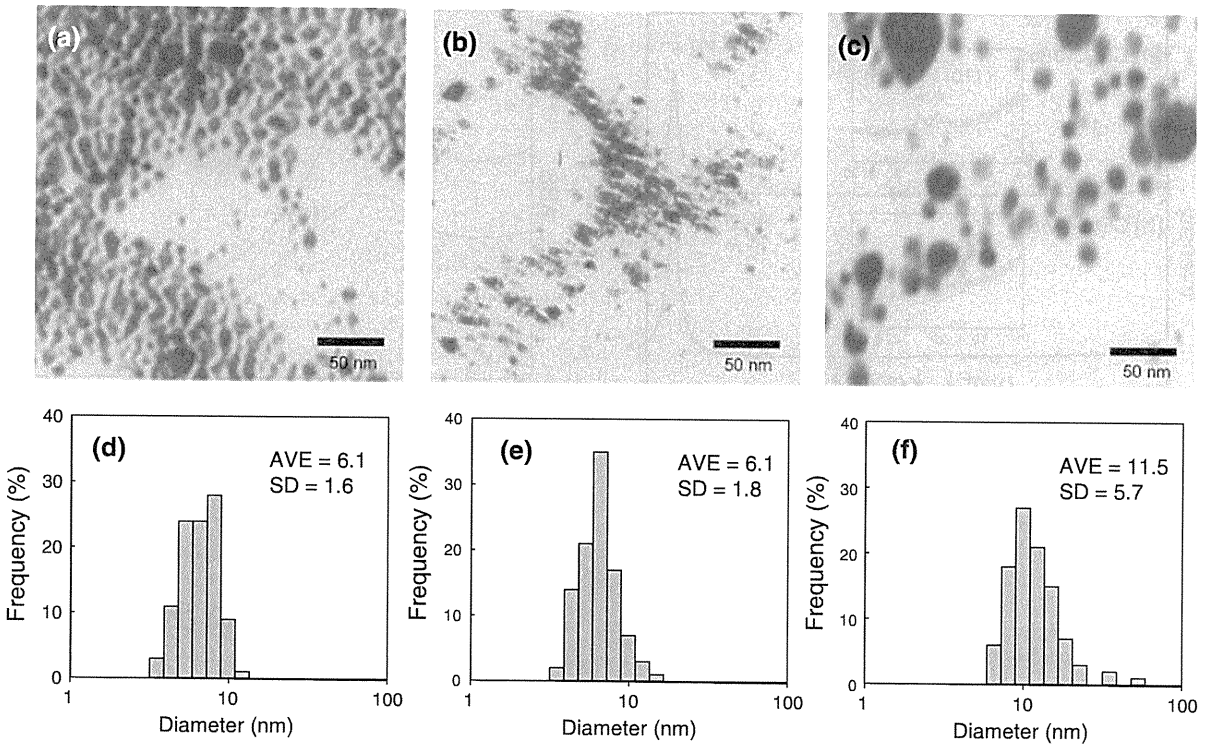

Fig. 3 TEM images and size distributions of **a** and **d** CELL2Au, **b** and **e** CELL13Au, **c** and **f** CELL41Au

Table 1 Characteristics of CTAAu and CELLAu nanoparticles

Samples	Diameter of Au core (d) (nm)[a]		Theoretical length of cellulosic chains (l) (nm)[b]	Composition of cellulosic chains in CTAAu and CELLAu (wt%)[c]	Interchain distance of cellulosic chains (Å)[c]	Calculated diameter of CTAAu and CELLAu ($D_{calc.}$) (nm)[d]	Hydrodynamic diameter of CTAAu and CELLAu (D) (nm)[e]
	AVE	SD					
CTA2Au	8.7	1.4	2.0	15.7	5.1	12.7	16.6
CTA13Au	7.9	3.2	7.5	22.7	9.5	22.9	49.0
CTA41Au	13.4	6.3	21.5	35.1	9.3	56.4	69.5
CELL2Au	6.1	1.6	2.0	9.5	5.1	10.1	21.8
CELL13Au	6.1	1.8	7.5	14.2	9.5	21.1	55.9
CELL41Au	11.5	5.7	21.5	23.3	9.3	54.5	–

[a] Determined by TEM analysis. *AVE* average, *SD* standard deviation

[b] Theoretical values of CTAS chain in streched conformation. The length of lipoyl chain in all-trans conformation = 1.0 nm

[c] Values of CELLAus were calculated from those of CTAAus determined in Ref (Enomoto-Rogers et al. 2010)

[d] $D_{calc.} = d + 2\,l$

[e] Determined by DLS measurements

cellulose II, or anti-parallel cellulose chains might be formed by interdigitation of cellulose chains on the gold and give diffraction pattern of cellulose II. Therefore, it was hard to discuss the mechanism of formation of cellulose II crystalline structure in relation to the orientation of cellulose chains in self-assembled structures. CELL41Au showed weak amorphous pattern of cellulose as shown in Fig. 4b. According to the contents of CTAS chains in CTAAu calculated in our previous work (Enomoto-Rogers

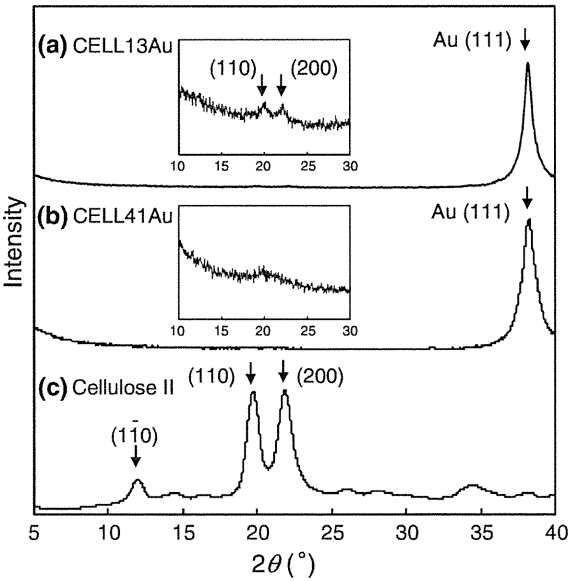

Fig. 4 Wide angle X-ray diffractgrams of **a** CELL13Au, **b** CELL41Au, and **c** cellulose II

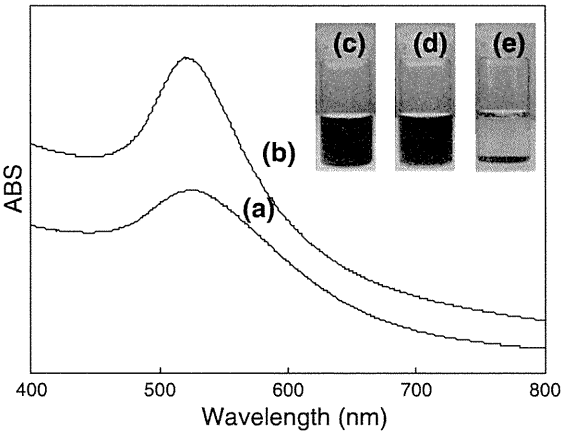

Fig. 5 UV–vis spectra of **a** CELL2Au and **b** CELL13Au in water (0.1 mg/mL), and images of **c** CELL2Au, **d** CELL13Au, and **e** CELL41Au in water

et al. 2010), the contents of cellulose chains in CELL13Au and CELL41Au were calculated to be 14.2 and 23.3 wt%, respectively as listed in Table 1. However, crystallinity of cellulose chains on the gold nanoparticles was low. The interchain distances of cellulose chains on the gold surface of CELL13Au and CELL41Au were calculated to be 9.5 and 9.3 Å, respectively, according to the our previous work on CTA13Au and CTA41Au (Enomoto-Rogers et al. 2010). Those values were both longer than the interchain distances of cellulose chains in crystal lattice of cellulose I (I_α: $a = 6.74$ Å, $b = 5.93$ Å, $c = 10.36$ Å, I_β: $a = 8.20$ Å, $b = 7.78$ Å, $c = 10.34$ Å) (Sugiyama et al. 1991; Woodcock and Sarko 1980) or cellulose II ($a = 8.01$ Å, $b = 9.04$ Å, $c = 10.36$ Å) (Kolpak and Blackwell 1976). The reason for amorphous pattern of cellulose on the surface of gold nanoparticles is likely that crystallization of cellulose chains via hydrogen bonding was inhibited by their covalent grafting on the gold surface at the longer interchain distances than those suitable for the crystallization. This low crystallinity of cellulose chains probably allowed water to interact with hydroxyl groups of cellulose chains, and dispersed CELL13Au in water. Therefore, nano-dispersity and solubility of these amorphous cellulose chains on the surface of gold nanoparticles were investigated in the following sections.

Nanostructures of CELL2Au and CELL13Au in water

The UV–vis spectra and the images of the gold nanoparticles CELL2Au and CELL13Au in water are shown in Fig. 5. The absorption band at λ = ca. 530 nm in UV–vis spectra are assigned to the surface plasmon band of gold (Brust and Kiely 2002), indicating that the gold were well-dispersed in nano-scale. CELL41Au nanoparticles were not dispersed in water, probably due to stronger hydrogen bonding between cellulose chains with higher molecular weight.

The hydrodynamic diameters (D) of CELL2Au and CELL13Au nanoparticles in water were determined by DLS measurements, and listed in Table 1. The intensity and number size distributions of CELL2Au and CELL13Au were shown in Fig. 6. The hydrodynamic diameter indicates the total diameter of nanoparticles with the gold core and cellulose shell. The hydrodynamic diameters (D) of CTA2Au and CTA13Au in chloroform were 16.6 and 49.0 nm, respectively as discussed in previous work (Enomoto-Rogers et al. 2010). The hydrodynamic diameters (D) of CELL2Au and CELL13Au in water were 21.8 and 55.9 nm, respectively. Generally, in DLS measurement, the larger particles exhibit much stronger intensity even when their number is very small. In the number size distribution, the number of particles around 10 nm is much larger than that around 100 nm, as shown in Fig. 6d. We consider

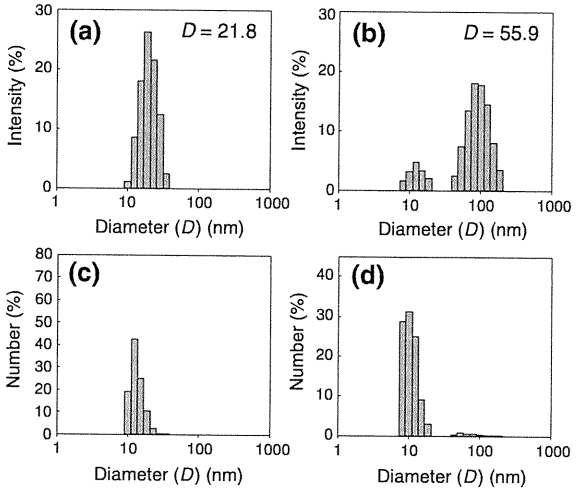

Fig. 6 Intensity size distributions of **a** CELL2Au and **b** CELL13Au, and number size distributions of **c** CELL2Au and **d** CELL13Au, in water (1.0 mg/mL)

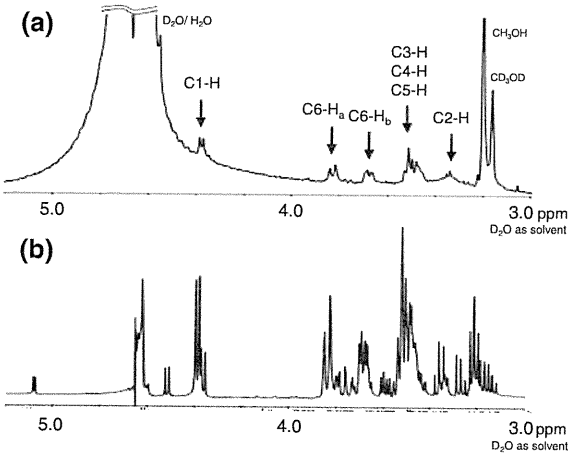

Fig. 7 ^{1}H-NMR spectra of **a** CELL13Au and **b** cellohexaose in deuterium oxide (D_2O)

that the bimodal distribution of intensity is just a result of analysis of scattering data calculated by Marquardt method. Although the solvents are different, the D values showed no substantial difference before and after deacetylation, indicating that the gold nanoparticles were well-dispersed in nano-scale. Consequently, these experiments revealed that the cellulose chains bound covalently on the gold surface in a radial manner.

Solubility of cellulose chains (DP_n = 13) on the surface of gold nanoparticles in water

Chemical structure of low-molecular-weight cellulose chains (DP_n = 13) on the gold nanoparticles was analyzed by NMR measurements. ^{1}H-NMR spectrum of CELL13Au in deuterium oxide (D_2O) is shown in Fig. 7. The proton resonances appeared at δ 4.38 (d, $J_{1,\,2}$ = 8, C1–H), 3.83 (dd, $J_{6a,\,6b}$ = 12, $J_{5,\,6a}$ = 2, C6–H_a), and 3.68 (dd, $J_{6a,\,6b}$ = 12, $J_{5,\,6b}$ = 4, C6–H_b) ppm, although their peak intensities were low. The observed peaks were identical to ring-proton peaks of low-molecular-weight cellulose (DP_n = 15) in 4% NaOD/D_2O solution (Isogai 1997). It has been reported that mono- or di-saccharides linked on the gold nanoparticles were water-soluble and could be analyzed by ^{1}H-NMR measurements (de la Fuente et al. 2001; Ojeda et al. 2007). It has also been reported that cellulose with DP of more than ca. 8 are not water-soluble (Kobayashi et al. 1991). The proton peaks of CELL13Au were different from those of cellohexaose (DP = 6), as shown in Fig. 7b. Low-molecular-weight cellulose (DP_n = 13) itself that was crystallized via inter- and intra- molecular hydrogen bonding was insoluble in water. Thus, low-molecular-weight cellulose chains (DP_n = 13) on the surface of gold nanoparticles were found to "dissolve" in water including a trace of methanol under the neutral condition.

It is likely that crystallization of cellulose chains (DP_n = 13) via hydrogen bonding was inhibited by covalent bonding of cellulose on the gold nanoparticles with wider interchain distances compared to crystal lattices of cellulose I or cellulose II. Interaction between cellulose chains and water molecules might be accelerated. As a result, the solubility of cellulose chains (DP_n = 13) in water was induced.

Conclusions

Cellulose chains self-assembled on the surface of gold nanoparticles, CELL2Au, CELL13Au, and CELL41Au were prepared. CELL2Au and CELL13Au were well-dispersed in water with a trace of methanol, while CELL41Au was not. Cellulose chains on the surface of gold nanoparticles were mostly amorphous according to the TEM observation and the XRD measurements. The UV–vis and DLS spectra of CELL2Au and CELL13Au in water

revealed that cellulose chains on the gold were organized in a radial manner with head-to-tail orientation. ^{1}H-NMR measurement revealed that cellulose chains ($DP_n = 13$) on the gold nanoparticles dissolved in water. Crystallization of cellulose chains ($DP_n = 13$) was inhibited because of their wide interchain distance on the gold surface. As a result, their solubility in water was induced.

Acknowledgments We acknowledge Advanced Instrumental Analysis Unit, Graduate School of Agricultural and Life Sciences, the University of Tokyo, for measuring a 500-MHz ^{1}H-NMR spectrum. This study was supported in part by a Grant-in-Aid from a Research Fellowships of the Japan Society for the Promotion of Science (JSPS) for Young Scientists (Y.E-R), and by a Grant-in-Aid for Scientific Research from the Ministry of Education, Science, and Culture of Japan (Nos. 18688009 and 21580205).

References

Atalla RH, Ellia JD, Schroeder LR (1984) Some effects of elevated temperatures on the structure of cellulose and its transformation. J Wood Chem Technol 4:465–482

Brust M, Kiely CJ (2002) Some recent advances in nanostructure preparation from gold and silver particles: a short topical review. Colloids Surf A Physicochem Eng Asp 202:175–186

de la Fuente JM, Barrientos AG, Rojas TC, Rojo J, Canada J, Fernandez A, Penades S (2001) Gold glyconanoparticles as water-soluble polyvalent models to study carbohydrate interactions. Angew Chem Int Ed 40:2257–2261

Enomoto Y, Kamitakahara H, Takano T, Nakatsubo F (2006) Synthesis of diblock copolymers with cellulose derivatives. 3. Cellulose derivatives carrying a single pyrene group at the reducing-end and fluorescent studies of their self-assembly systems in aqueous NaOH solutions. Cellulose 13:437–448

Enomoto-Rogers Y, Kamitakahara H, Nakayama K, Takano T, Nakatsubo F (2009a) Synthesis and thermal properties of poly (methyl methacrylate)-*graft*-(cellobiosylamine-c15). Cellulose 16:519–530

Enomoto-Rogers Y, Kamitakahara H, Takano T, Nakatsubo F (2009b) Cellulosic graft copolymer: Poly (methyl methacrylate) with cellulose side chains. Biomacromolecules 10:2110–2117

Enomoto-Rogers Y, Kamitakahara H, Yoshinaga A, Takano T (2010) Radially oriented cellulose triacetate chains on gold nanoparticles. Cellulose 17:923–936

Gulari E, Gulari E, Tsunashima Y, Chu B (1979) Photon-correlation spectroscopy of particle distributions. J Chem Phys 70:3965–3972

Isogai A (1997) NMR analysis of cellulose dissolved in aqueous NaOH solutions. Cellulose 4:99–107

Isogai A, Usuda M (1991) Preparation of low-molecular-weight celluloses using phosphoric-acid. Mokuzai Gakkaishi 37:339–344

Isogai A, Usuda M, Kato T, Uryu T, Atalla RH (1989) Solid-state cp mas c13 NMR-study of cellulose polymorphs. Macromolecules 22:3168–3172

Kamide K, Okajima K, Kowsaka K (1992) Dissolution of natural cellulose into aqueous alkali solution—role of super-molecular structure of cellulose. Polym J 24:71–86

Kamitakahara H, Nakatsubo F (2005) Synthesis of diblock copolymers with cellulose derivatives. 1. Model study with azidoalkyl carboxylic acid and cellobiosylamine derivative. Cellulose 12:209–219

Kamitakahara H, Enomoto Y, Hasegawa C, Nakatsubo F (2005) Synthesis of diblock copolymers with cellulose derivatives. 2. Characterization and thermal properties of cellulose triacetate-block-oligoamide-15. Cellulose 12:527–541

Kobayashi S, Kashiwa K, Kawasaki T, Shoda S (1991) Novel method for polysaccharide synthesis using an enzyme - the 1st invitro synthesis of cellulose via a nonbiosynthetic path utilizing cellulase as catalyst. J Am Chem Soc 113:3079–3084

Kolpak FJ, Blackwell J (1976) Determination of structure of cellulose II. Macromolecules 9:273–278

Ojeda R, de Paz JL, Barrientos AG, Martin-Lomas M, Penades S (2007) Preparation of multifunctional glyconanoparticles as a platform for potential carbohydrate-based anticancer vaccines. Carbohydr Res 342:448–459

Qazi SJS, Rennie AR, Cockcroft JK, Vickers M (2009) Use of wide-angle x-ray diffraction to measure shape and size of dispersed colloidal particles. J Colloid Interf Sci 338:105–110

Sugiyama J, Vuong R, Chanzy H (1991) Electron-diffraction study on the 2 crystalline phases occurring in native cellulose from an algal cell-wall. Macromolecules 24:4168–4175

Wang SH, Sato S, Kimura K (2003) Preparation of hexagonal-close-packed colloidal crystals of hydrophilic monodisperse gold nanoparticles in bulk aqueous solution. Chem Mater 15:2445–2448

Wang N, Ding EY, Cheng RS (2007) Thermal degradation behaviors of spherical cellulose nanocrystals with sulfate groups. Polymer 48:3486–3493

Wang N, Ding E, Cheng RS (2008) Preparation and liquid crystalline properties of spherical cellulose nanocrystals. Langmuir 24:5–8

Woodcock C, Sarko A (1980) Packing analysis of carbohydrates and polysaccharides.11. Molecular and crystal-structure of native ramie cellulose. Macromolecules 13:1183–1187

Cellulose (2011) 18:1005–1014
DOI 10.1007/s10570-011-9549-4

Synthesis of diblock copolymers with cellulose derivatives 4. Self-assembled nanoparticles of amphiphilic cellulose derivatives carrying a single pyrene group at the reducing-end

Yukiko Enomoto-Rogers · Hiroshi Kamitakahara · Arata Yoshinaga · Toshiyuki Takano

Received: 1 December 2010 / Accepted: 15 April 2011 / Published online: 3 May 2011
© Springer Science+Business Media B.V. 2011

Abstract Self-assembled cellulose-pyrene nanoparticles were prepared from amphiphilic cellulose derivatives carrying a single pyrene group at the reducing-end, *N*-(1-pyrenebutyloyl)-β-cellulosylamine (CELL13Py and CELL30Py, the number average degrees of polymerization (DP_n) of 13 and 30, respectively) and *N*-(15-(1-pyrenebutyloylamino)-pentadecanoyl)-β-cellulosylamine (CELL13C15Py and CELL30C15Py, DP_n of 13 and 30, respectively). Transmission electron microscopy (TEM) observation revealed that CELL13C15Py and CELL30C15Py formed self-assembled nanoparticles with the average diameters of 108.8 and 40.0 nm, respectively. The average radius of CELL30C15Py nanoparticles (20.0 nm) agreed well with the molecular length of its cellulose chain (19.2 nm). CELL30C15Py nanoparticles were expected to have monolayered structure, consisting of cellulose shell with radial orientation and hydrophobic core of 15-(1-pyrenebutyloylamino)-pentadecanoyl groups. The fluorescent spectrum of CELL30C15Py nanoparticles showed an excimer emission due to dimerized pyrene groups, indicating that the pyrene groups at the reducing-end of cellulose are associating in the particles. The balance of hydrophilic and hydrophobic parts of the cellulose derivatives controlled their self-assembled nanostructures. X-ray diffraction measurements revealed that radially oriented cellulose chains of CELL30C15Py nanoparticles were mostly amorphous, and at the same time exhibited weak reflection pattern of cellulose II, which is believed to have anti-parallel orientation.

Keywords Cellulose · Reducing-end · Nanoparticle · Self-assembly · Radial orientation · Fluorescent probe technique · Pyrene

Y. Enomoto-Rogers · H. Kamitakahara (✉) · A. Yoshinaga · T. Takano
Division of Forest and Biomaterials Science, Graduate School of Agriculture, Kyoto University, Kitashirakawa-Oiwake-cho, Sakyo-ku, Kyoto 606-8502, Japan
e-mail: hkamitan@kais.kyoto-u.ac.jp

Introduction

Cellulose is a linear (1→4)-β-glucopyranan having three hydroxyl groups at C2, C3, and C6 positions per anhydro glucose unit. The cellulose molecule has only one hemiacetal hydroxyl group at the reducing-end, which can be substituted with other functional groups with high regioselectivity. Focusing on the specific reactivity of the reducing-end group, we have succeeded to prepare cellulosic diblock copolymers by introducing long-chain alkyl groups into the reducing-end of cellulose chain (Kamitakahara et al. 2005; Kamitakahara and Nakatsubo 2005). Based on the same synthetic strategy, we have prepared copolymers with cellulose side-chains (Enomoto-Rogers et al. 2009a; Enomoto-Rogers et al. 2009b) and cellulose triacetate

self-assembled gold nanoparticles (Enomoto-Rogers et al. 2010) to control self-assembly and orientation of cellulose chains. However, cellulose nanoparticles with radial orientation have not prepared yet, and their properties such as crystallinity are still unknown.

One of the most common nanoscaled cellulose materials is cellulose nanocrystal, which can be prepared by acid hydrolysis (Habibi et al. 2010). The cellulose nanocrystal is usually needle-shaped bundle of cellulose chains, and its size is 5–20 nm wide and 100–2,000 nm long. There have also been a few studies on sphere-shaped cellulose nanocrystal (Wang et al. 2008; Wang et al. 2007). The crystalline structure of these cellulose nanocrystals is the same as that of the original fibers, cellulose I in native form. Self-assembled cellulose nanoparticles organized in a radial manner with head-to-tail orientation have fundamentally different structure from cellulose nanocrystal prepared from native cellulose.

In general, cellulose I, the native form, is believed to have parallel orientation (Gardner and Blackwel 1974; Sugiyama et al. 1991). On the other hand, cellulose II, the regenerated or mercellized form, is believed to have anti-parallel orientation (Kolpak and Blackwell 1976; Langan et al. 1999). Cellulose crystals with parallel orientation have not yet been prepared in the solid state from regenerated cellulose or by chemical synthesis, although there have been some attempts using cello-oligosaccharide analogues (Bernet et al. 2000; Murty et al. 2006). Therefore, structure of cellulose chains organized in a radial manner with head-to-tail orientation is of considerable fundamental interest.

Recently, we have prepared amphiphilic cellulosic derivatives carrying a single pyrene group as a probe at the reducing-end. Fluorescent properties of pyrene revealed that these cellulose derivatives were self-assembled in NaOH aqueous solutions (Enomoto et al. 2006). The self-assembled cellulosic derivatives should have cellulose shell and hydrophobic core structure, where cellulose chains are oriented in a parallel or a radial manner. In the present report, we demonstrated the method to prepare self-assembled nanoparticles of amphiphilic cellulose derivatives carrying a long-chain alkyl group and a pyrene group. Effect of hydrophobic-hydrophilic balance of the compounds on their self-assembly systems and nanostructures were investigated by means of transmission electron microscopy (TEM) observations and fluorescent measurements.

Experimental

General measurements

^{1}H-, ^{13}C-, and two-dimensional NMR spectra were recorded on a JEOL JNM-A500 FT-NMR (500 MHz) spectrometer, in $CDCl_3$ with tetramethylsilane (TMS) as an internal standard. Chemical shifts (δ) and coupling constants (J) are reported in (ppm) and (Hz), respectively. Fourier transform infrared (FT-IR) spectra were recorded on a Shimadzu FTIR-4000 spectrophotometer equipped with an ATR attachment (DuraSampl IR-II).

GPC measurement

Number and weight average molecular weights (M_n and M_w) and polydispersity index (M_w/M_n) were estimated by gel permeation chromatography (GPC) (SCL-10Avp, SIL-10A, LC-10Ai, CTO-10ACvp, RID-10A, Shimadzu, Japan) in chloroform at 40°C. Shodex columns (K-806 M, K-802) were used. The flow rate was 0.8 mL/min. Calibration curves were obtained by using polystyrene standards (Shodex).

TEM analysis

Transmission electron microscopy (TEM) images were collected by JEOL JEM-1220 system operating at an accelerating voltage of 100 kV. The never-dried self-assembled cellulose-pyrene nanoparticles in methanol (ca. 0.1 mg/mL) were dispersed again by stirring, and a portion of the obtained suspension was deposited on copper grids that were pre-coated by Formvar (polyvinyl formal) and reinforced by carbon, and stained with uranyl diacetate (UA). The sizes of particles were calibrated using Latex Particles ϕ0.23 μm (Ohken Shoji, Japan). TEM images were recorded on Fuji FG films (Fuji Film, Japan). TEM images were analyzed using public domain ImageJ program (Rasband, W. S., U. S. National Institutes of Health, Bethesda, Maryland, USA, http://rsb.info.nih.gov/ij/, 1997–2009).

Fluorescent measurements

Steady-state fluorescence spectra were recorded on a Shimadzu RF-5300PC spectrofluorophotometer. The never-dried self-assembled cellulose-pyrene

nanoparticles in methanol (ca. 0.1 mg/mL) were dispersed again by stirring, and a portion of the obtained suspension was loaded into a fluorescence cell, and analyzed in 1 min before precipitation occurred. All measurements were carried out at 25 °C. They were recorded with an excitation wavelength of 350 nm. Excitation and emission slits were normally set at 5.0 nm. The excimer-to-monomer ratios (I_E/I_M) were calculated by taking the ratio of the emission intensity at ca. 470 nm to the half-sum of the emission intensities at 379 and 398 nm.

X-ray diffraction measurements

X-ray diffraction measurements were carried out with a Rigaku diffractometer Ultima IV. A Nickel-filtered CuKα radiation was used at 40 kV and 30 mA. Cellulose microcrystalline (Avicel, Merck) and low-molecular-weight cellulose was used to obtain reflection pattern of cellulose I and cellulose II, respectively.

Materials

N-(1-Pyrenebutyloyl)-tri-*O*-acetyl-β-cellulosylamine, CTA13Py (DP_n=13) and CTA30Py (DP_n = 30), and *N*-(15-(1-pyrenebutyloylamino)-pentadecanoyl)-tri-*O*-acetyl-β-cellulosylamine CTA13C15Py (DP_n = 13) and CTA30C15Py (DP_n = 30), cellulose triacetates (CTA13 (DP_n = 13) and CTA30 (DP_n = 30)) were prepared as described in the previous article (Enomoto et al. 2006; Kamitakahara et al. 2005). Number and weight average molecular weights (M_n and M_w) and polydispersity index (M_w/M_n) of acetylated cellulose derivatives were estimated by GPC measurements using polystyrene standards. Number average degrees of polymerization (DP_n) of cellulose chains of the derivatives were calculated from peak ratio of pyrene groups to ring protons in the ^{1}H-NMR spectra. The theoretical molecular lengths of cellulose derivatives were calculated from degrees of polymerization determined by NMR analysis. Low-molecular-weight cellulose (DP_n = 13) was prepared from cellulose microcrystalline (CF-11, Whatman) using phosphoric acid according to previous article (Atalla et al. 1984; Isogai and Usuda 1991). Cellulose microcrystalline (Avicel, Merck), cellulose microcrystalline (CF-11, Whatman), 1,8-diazabicyclo[5,4,0]-7-undecene (DBU) and all other reagents were commercially obtained and used without further purification.

N-(1-Pyrenebutyloyl)-β-cellulosylamine (CELL13Py and CELL30Py)

To a solution of *N*-(1-pyrenebutyloyl)-tri-*O*-acetyl-β-cellulosylamine, CTA13Py (DP_n = 13) (3.0 mg) in methanol/1,4-dioxane (1:4, 0.3 mL), DBU (30 μL, 0.02 mmol) was added at room temperature, and stirred for 4 h under the nitrogen. The precipitated compounds were washed with methanol to remove DBU, and then methanol and DBU were removed by decantation to avoid collapse of the particles. This procedure was repeated at least five times. The precipitated compounds were preserved in methanol. For sample preparation, the precipitated compounds in methanol were dispersed again by stirring, and a portion of the obtained suspension was loaded into a cell for fluorescent measurements or deposited on a copper grid for TEM observations. For X-ray analysis, methanol in the suspension of nanoparticles were replaced with water by decantation, and freeze-dried to obtain the powder of cellulose nanoparticles of *N*-(1-pyrenebutyloyl)-β-cellulosylamine, CELL13Py (DP_n = 13) (1.3 mg, 81.2%). The complete deacetylation of the cellulose derivatives was confirmed by FT-IR spectrum with disappearance of absorbance of acetyl group at 1,755 cm^{-1} (C = O) and appearance of absorbance of hydroxyl group at 3,400 cm^{-1} (OH). The same procedure was applied to CTA30Py (DP_n = 30) (3.0 mg), to give *N*-(1-pyrenebutyloyl)-β-cellulosylamine CELL30Py (DP_n = 30) (1.0 mg, 66.7%).

N-(15-(1-Pyrenebutyloylamino)-pentadecanoyl)-β-cellulosylamine (CELL13C15Py and CELL30C15Py)

The deprotection and self-assembly procedures described above were applied to *N*-(15-(1-pyrenebutyloylamino)-pentadecanoyl)-tri-*O*-acetyl-β-cellulosylamine, CTA13C15Py (DP_n = 13) (10.3 mg) and CTA30C15Py (DP_n = 30) (9.0 mg), to give cellulose nanoparticles of *N*-(15-(1-pyrene-butyloylamino)-pentadecanoyl)-β-cellulosylamine, CELL13C15Py (DP_n = 13) (2.8 mg, 50.0%) and CELL30C15Py (DP_n = 30) (2.7 mg, 54.0%), respectively.

Regenerated cellulose (CELL13 and CELL30)

CTA13 (DP_n = 13) (30.0 mg) and CTA30 (DP_n = 30) (30.0 mg) were deacetylated in the same manner described above to give regenerated cellulose, CELL13 (DP_n = 13) (9.8 mg, 58.3%) and CELL30 (DP_n = 30) (10.4 mg, 61.9%), respectively.

Results and discussion

Preparation of amphiphilic cellulose nanoparticles

Pyrene exhibits the monomer emission (intensity I_M, ca. 380 nm) when it is isolated from each other. Two pyrene molecules form excited dimer (excimer), and exhibit a broad structureless excimer emission (intensity I_E, ca. 480 nm) when they are associated in symmetrical sandwich arrangement at a distance of ca. 3.5 Å (Birks 1970). The formation of pyrene aggregate or hydrophobic domain can be confirmed by the presence of the pyrene excimer emission, and the ratio I_E/I_M can be used to evaluate the association system of pyrenes (Winnik et al. 1987). Diffusion and association of hydrophobic groups at the reducing-end of cellulose can be confirmed by the monomer and excimer emission of pyrenes, respectively, when a single pyrene group is regioselectively introduced to the reducing-end of the cellulose backbone.

Regarding a method to prepare self-assembled nanoparticles, nanoprecipitation is known as an effective way to prepare nanoparticles of amphiphilic polymers including cellulose esters or dextran esters out of organic/water solvent mixture, for example by dialysis or oil/water emultion method. (Hornig and Heinze 2008; Hornig et al. 2005; Kataoka et al. 2001; Lassalle and Ferreira 2007; O'Reilly et al. 2006). Amphiphilic cellulosic derivatives carrying a long-chain alkyl and pyrene groups were not soluble in common organic solvents, such as chloroform or *N,N*-dimethyl formamide, as reported in our previous article (Enomoto et al. 2006). We anticipated that nanoparticles of amphiphilic cellulosic derivatives could be prepared via deprotection of acetylated cellulose derivatives in an organic solvent and self-assembly of the resulting amphiphilic cellulose derivatives in a nonsolvent, such as methanol.

N-(1-Pyrenebutyloyl)-β-cellulosylamine (CELL13Py (DP_n = 13) and CELL30Py (DP_n = 30)) and *N*-(15-(1-pyrenebutyloylamino)-pentadecanoyl)-β-cellulosylamine (CELL13C15Py (DP_n = 13) and CELL30C15Py (DP_n = 30)) were prepared through the deprotection of corresponding acetylated derivatives with an alkaline reagent, DBU in methanol/1,4-dioxane (1:4) mixed solvent. Regenerated cellulose without hydrophobic groups, CELL13 and CELL30 were prepared from cellulose triacetate (DP_n = 13 and 30, respectively) in the same procedure as control experiments. The chemical structures of the cellulose derivatives are shown in Fig. 1. Characteristics of these cellulose derivatives are summarized in Table 1. The theoretical molecular lengths of cellulose derivatives were calculated from degrees of polymerization determined by NMR analysis of corresponding acetylated cellulose derivatives. The amide linkages between C1 and pentadecanoyl group (-C1-NH-CO-) and between pentadecanoyl group and pyrenebutyloyl group (-CH_2-NH-CO-$(CH_2)_3$-Py) are stable under the alkaline condition using DBU (Enomoto et al. 2006). The cellulose derivatives did not precipitate in the solvent system during the reaction, likely due to the ionization of hydroxyl groups of cellulose. Preparation of nanoparticles was carried out by a combination of deprotection and self-assembly of the cellulose derivatives. The reaction mixture of the cellulose derivatives in methanol/1,4-dioxane was added dropwise into a larger amount of methanol, which is a poor solvent for cellulose, and allowed to stand overnight. The deprotected cellulose derivatives precipitated as nanoparticles, as discussed in the next sections, through a quite slow self-assembly in methanol. When the deprotection was carried out using sodium methoxide as an alkaline reagent in methanol/

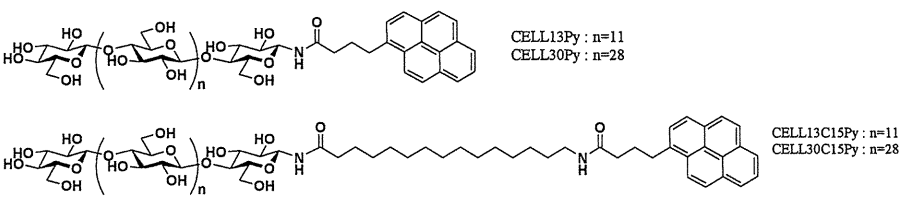

Fig. 1 Chemical structures of cellulose derivatives, CELL13Py, CELL13C15Py, CELL30Py, and CELL30C15Py

Table 1 Characteritics of regenerated cellulose and cellulose derivatives

Cellulose derivatives	M_n $(10^{-4})^a$	PDI[a]	DP_n of cellulose chain calculated from M_n^a	DP_n of cellulose chain calculated by NMR analysis[b]	Theoretical molecular length of cellulose chain (nm)[c]	Theoretical molecular length of one molecule (nm)[e]
CELL13	0.37	1.30	13	–	6.4[d]	6.4
CELL13Py	0.47	1.40	15	11	5.5	6.7
CELL13C15Py	0.48	1.50	15	12	6.0	9.4
CELL30	0.85	1.83	30	–	15.0[d]	15.0
CELL30Py	1.18	1.81	40	27	13.5	14.7
CELL30C15Py	1.28	1.75	43	32	15.8	19.2

[a] Number average molecular weight and polydispersity index (PDI) of acetylated derivatives calculated by GPC analysis using PS standards. [b]Calculated from integral areas of ring-protons and pyrene aromatic protons of the acetylated derivatives. [c]Calculated from DP_n determined by NMR analysis. [d]Calculated from DP_n determined by GPC analysis. [e]Including long-chain alkyl and pyrene groups in all-*trans* conformation

chloroform, the deprotected derivatives precipitated as disordered and irregular aggregates in few hours. The precipitates of deprotected cellulose derivatives were washed with methanol, and methanol and DBU were removed by decantation. Those precipitates were insoluble and not dispersed as colloids in water or other common organic solvents such as *N*,*N*-dimethyl formamide or dimethyl sulfoxide, and never formed suspension again in methanol or water when they were dried. The samples for TEM analysis and fluorescent measurements were prepared from the suspension of never-dried cellulose derivatives.

Nanostructures of self-assembled cellulose-pyrene nanoparticles

Nanostructures of the cellulose derivatives were analyzed by TEM. The TEM images of cellulose and cellulose derivatives are shown in Fig. 2. CELL13, CELL13Py, CELL30, and CELL30Py formed irregular aggregates, which were positively stained with UA, as shown in Fig. 2a, b, e, and d, respectively. However, in the case of cellulose derivatives carrying long-chain alkyl and pyrene groups, CELL13C15Py and CELL30C15Py, the nanoparticles were observed as shown in Fig. 2c, f. These nanoparticles were negatively stained with UA, suggesting crystallization or stronger packing of cellulose chains, compared to other irregular aggregates of cellulose. The size distribution histograms, average diameter (AVE), and standard deviation (SD) of CELL13C15Py and CELL30C15Py obtained by TEM analysis are shown in Fig. 3. The CELL13C15Py and CELL30C15Py nanoparticles tended not to disperse individually on a copper grid due to a strong interaction between particles, resulting in the production of large interparticle aggregates. Consequently, we found the well-dispersed particles as shown in Fig. 2c, f. The well-dispersed particles exist in the top half of Fig. 2f, and the interparticle aggregates exist in the bottom half and the black-colored bottom end of Fig. 2f. Due to low contrast of the aggregates, we could not identify sufficient number of the particles to measure their size, and, as a result, could not calculate their deviation. However, we confirmed the reproducibility of data obtained by fluorescent and XRD measurements. This fact also supports the reproducibility of the structure of the cellulosic nanoparticles. The same phenomena such as interparticle aggregation is reported in previous articles on spherical cellulose nanocrystals prepared by hydrolysis of cellulose microcrystals (Wang et al. 2008; Wang et al. 2007). The suspension of the cellulose nanoparticles obtained in this study was stable in methanol after a couple of months.

The average diameter of CELL13C15Py nanoparticles was 108.8 nm. The edge of particles was clearly stained, suggesting a strong packing of cellulose chains or stability of the nanoparticles. It was suggested that CELL13C15Py formed self-assembled nanoparticles due to hydrophobic interactions between 15-(1-pyrenebutyloylamino)-pentadecanoyl groups. No hollow was observed in TEM images of CELL13C15Py nanoparticles. In addition, the theoretical molecular length of CELL13C15Py is

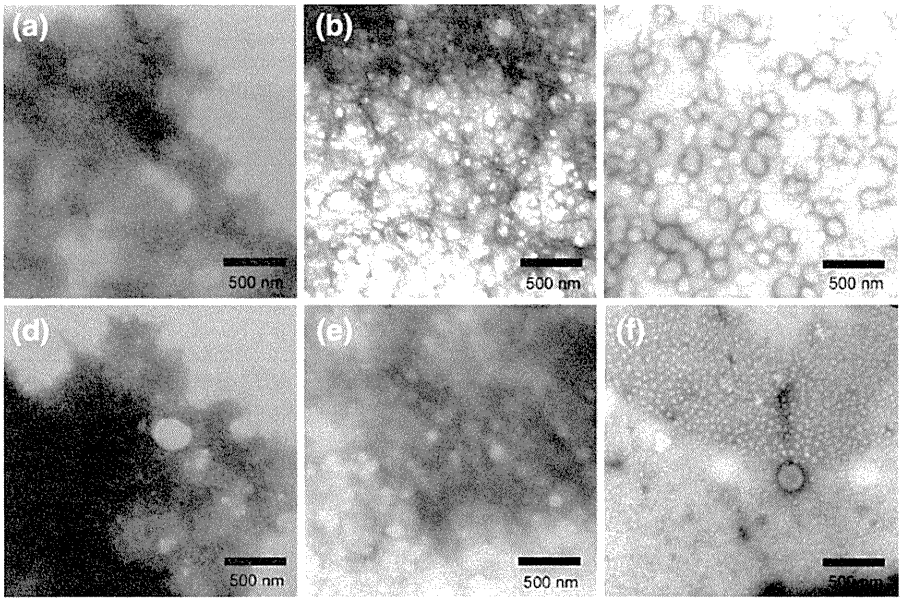

Fig. 2 TEM images of **a** CELL13, **b** CELL13Py, **c** CELL13C15Py, **d** CELL30, **e** CELL30Py, and **f** CELL30C15Py dispersed in methanol

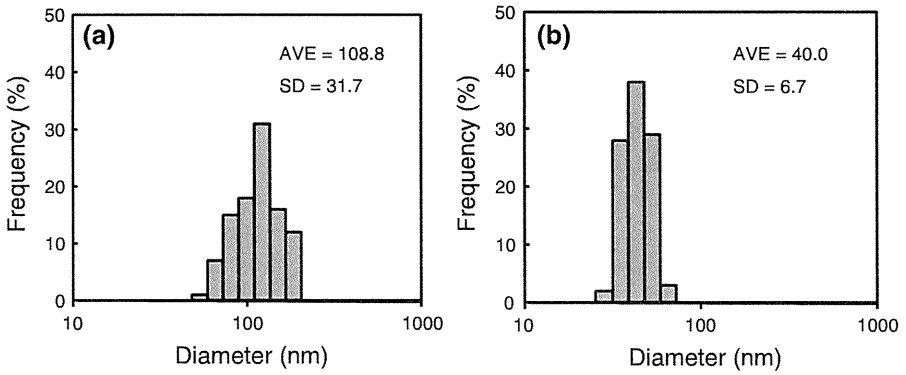

Fig. 3 Size distributions of the diameters of **a** CELL13C15Py and **b** CELL30C15Py, analyzed by TEM observation

9.4 nm, and this value is rather smaller than the radius of CELL13C15Py nanoparticles (54.4 nm) as shown in Fig. 2c. Consequently, it was suggested that CELL13C15Py nanoparticles were not monolayered. It was, however, difficult to investigate further detailed structures inside the nanoparticle.

CELL30C15Py formed smaller nanoparticles with the average diameter of 40.0 nm compared to CELL13C15Py nanoparticles, and the standard deviation of their diameters was smaller than that of CELL13C15Py. The enlarged image of Fig. 2f is shown in Fig. 4a. The theoretical molecular length of CELL30C15Py was calculated to be 19.2 nm. The radius of CELL30C15Py nanoparticles (20.0 nm) agreed well with its molecular length. It was suggested that CELL30C15Py nanoparticles were monolayered, consisting of cellulose shell with radial orientation and hydrophobic core of long-chain alkyl group. Pyrene group should be located inside of the hydrophobic domain. The structural image of a single cellulose nanoparticle of CELL30C15Py was illustrated in Fig. 4b. The deviations of diameter of nanoparticles are likely due to the polydispersity of cellulose chains. Consequently, the novel self-assembled nanoparticles of amphiphilic cellulose derivatives were successfully prepared through the deprotection of acetyl groups under alkaline condition and the subsequent slow self-assembly. A

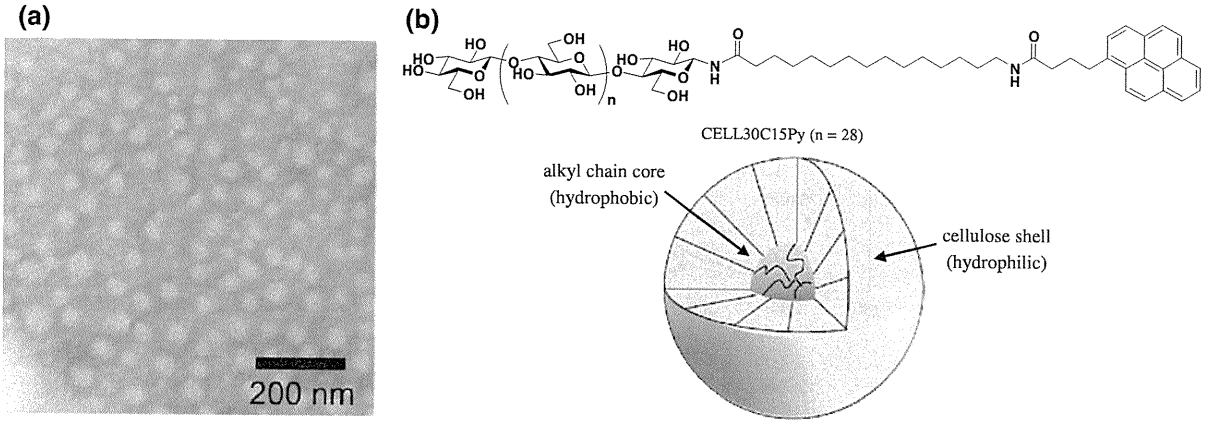

Fig. 4 **a** Enlarged TEM image of Fig. 2f and **b** structural image of CELL30C15Py nanoparticle

hydrophilic-hydrophobic balance in one molecule controlled their self-assembled nanostructures.

Fluorescent studies of self-assembled cellulose-pyrene nanoparticles

The association system of self-assembled cellulose-pyrene nanoparticles was investigated by means of the fluorescent probe method. Fluorescence spectra of the suspension of the never-dried self-assembled cellulose-pyrene nanoparticles in methanol were measured after the nanoprecipitation and removal of DBU. The fluorescence spectra of the cellulose derivatives are shown in Fig. 5. The CELL13Py and CELL30Py showed the strong monomer emission (at ca. 380 and 390 nm) due to a locally excited pyrene, as shown in Fig. 5a, c. The I_E/I_M values of CELL13Py (I_E/I_M = 0.18) and CELL30Py (I_E/I_M = 0.11) remained low, indicating that the pyrenes of these derivatives diffused and did not associate.

On the other hand, CELL13C15Py and CELL30C15Py having a long-chain alkyl group, exhibited the excimer emission due to pyrene dimer (at ca. 470 nm) besides the monomer emission, as shown in Fig. 5b, d. The I_E/I_M values of CELL13C15Py (I_E/I_M = 0.41) and CELL30C15Py (I_E/I_M = 0.23) took higher values, compared to CELL13Py (I_E/I_M = 0.18) and CELL30Py (I_E/I_M = 0.11). The spectra imply that hydrophobic alkyl and pyrene groups at the reducing-end of CELL13C15Py and CELL30C15Py associated in the nanoparticles. The excimer emission of CELL13C15Py and CELL30C15Py are assigned to stronger hydrophobic interactions of pyrene groups

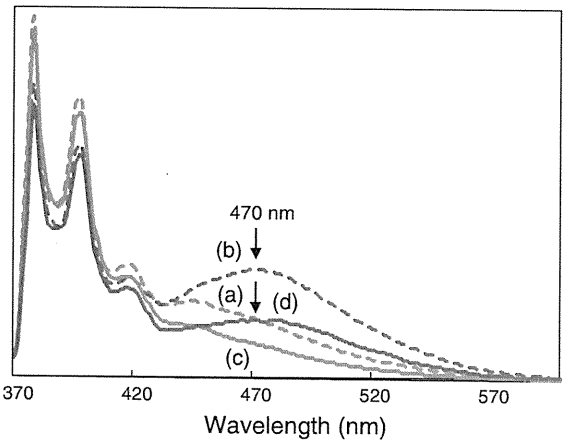

Fig. 5 Fluorescence spectra of pyrene of **a** CELL13Py, **b** CELL13C15Py, **c** CELL30Py, and **d** CELL30C15Py. 0.1 mg/mL in methanol. λ_{ex} = 350 nm, 25 °C

anchored at the end of long-chain alkyl group, compared to CELL13Py or CELL30Py. The CELL13C15Py, with higher composition of hydrophobic groups in the molecule, took higher I_E/I_M value, and formed larger nanoparticles than those in CELL30C15Py as shown in TEM images in Fig. 2c. Namely, more pyrene groups associated in the nanoparticles of CELL13C15Py with relatively stronger hydrophobic interactions, compared to those in CELL30C15Py nanoparticles.

Excimer emission of pyrenes originates from a "dynamic" pyrene dimer due to two pyrene molecules which are in collision with each other when excited, or a "static" pyrene dimer due to the pyrenes associated prior to excitation (Birks 1970). In general, for dynamic excimers, excitation spectra for the monomer (monitored at ca. 380 nm) and the excimer (monitored

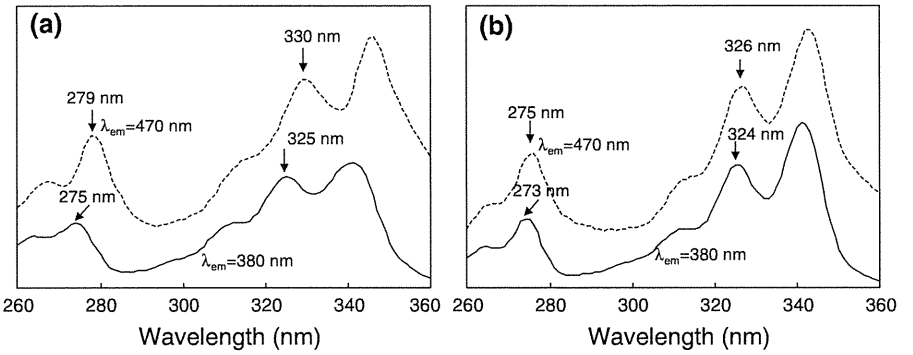

Fig. 6 Excitation spectra of **a** CELL13C15Py and **b** CELL30C15Py in methanol monitored at 380 nm (monomer) (*solid line*) and at 470 nm (excimer) (*dashed line*)

at ca. 470 nm) show the same peak patterns and positions. However, for "static" preassociated pyrene excimers which is formed before excitation, the spectrum for the excimer emission shows red-shift (ca. 1–8 nm) compared with that for the monomer emission, although they are identical in band patterns (Winnik 1990; Winnik et al. 1987; Winnik et al. 1998). The excitation spectra of CELL13C15Py and CELL30C15Py were measured to distinguish the origin of the excimer emission, and are shown in Fig. 6. The spectrum for the excimer monitored at 470 nm showed red-shift of ca. 2–5 nm, compared to that for the monomer monitored at 380 nm. Those facts indicated that the excimer emission of CELL13C15Py and CELL30C15Py originated from the "static" pyrene dimers (preassociated aggregates), not from the "dynamic" pyrene dimers. Those spectra, in the cases of CELL13C15Py and CELL30C15Py, support that those amphiphilic cellulose derivatives self-assembled to form nanoparticles promoted by the hydrophobic interaction between 15-(1-pyrenebutyloylamino)-pentadecanoyl groups.

X-ray diffraction measurements

In general, cellulose I, the native form, is believed to have parallel orientation. (Gardner and Blackwel 1974; Sugiyama et al. 1991). On the other hand, cellulose II, the regenerated or mercellized form, is believed to have anti-parallel orientation (Kolpak and Blackwell 1976; Langan et al. 1999). X-ray diffraction measurements were carried out to analyze crystalline pattern of self-assembled cellulose-pyrene nanoparticles. The diffraction angle and *d* spacings of cellulose and self-assembled cellulose-pyrene nanoparticles are summarized in Table 2. Cellulose chains of all derivatives had quite low crystallinity as shown in Fig. 7. CELL30 and

Table 2 Diffraction angle and *d* spacings of cellulose and self-assembled cellulose-pyrene nanoparticles

Samples	(1–10)		(110)		(200)	
	$2\theta^a$	d^b	$2\theta^a$	d^b	$2\theta^a$	d^b
CELL13	–	–	20.0	0.444	22.1	0.403
CELL13Py	12.2	0.724	19.9	0.447	21.9	0.406
CELL13C15Py	–	–	19.7	0.450	21.8	0.408
CELL30	–	–	–	–	–	–
CELL30Py	–	–	20.0	0.444	21.9	0.404
CELL30C15Py	–	–	19.8	0.448	21.8	0.407
Cellulose I	14.8	0.600	16.2	0.547	22.5	0.394
Cellulose II	12.0	0.739	19.7	0.451	21.8	0.407

[a] Diffraction angle (°). [b] *d* spacing (nm)

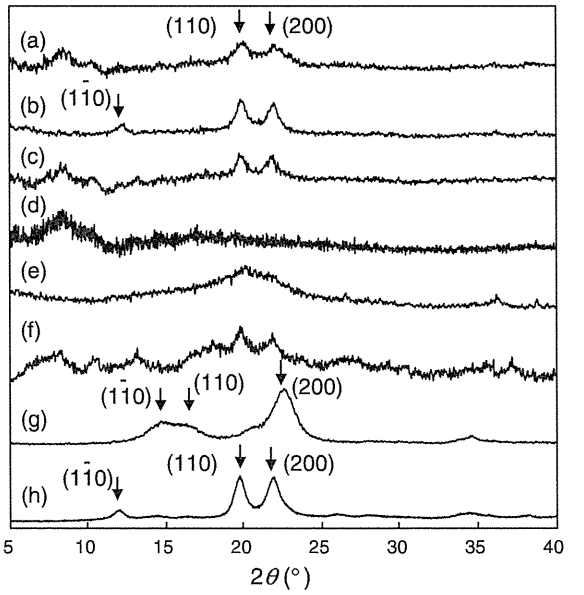

Fig. 7 Wide angle X-ray diffractgrams of **a** CELL13, **b** CELL13Py, **c** CELL13C15Py, **d** CELL30, **e** CELL30Py, **f** CELL30C15Py, **g** microcrystalline cellulose (cellulose I), and **h** regenerated cellulose (cellulose II)